Soft Matter

PAPER

View Article Online
View Journal | View Issue

Cite this: *Soft Matter*, 2023, **19**, 6329

Template-induced crystallization of charged colloids: a molecular dynamics study

Wenze Ouyang, *[a] Shuangyang Zou, [a] Jun Zhong[b] and Shenghua Xu*[ac]

Received 3rd July 2023,
Accepted 31st July 2023

DOI: 10.1039/d3sm00872j

rsc.li/soft-matter-journal

By using a large enough number of particles and implementing a parallel algorithm on the CUDA platform, we have performed brute-force molecular dynamics simulations to study the template-induced heterogeneous crystallization in charged colloids. Six kinds of templates, whose patterns include the planes of fcc(100), fcc(110), fcc(111), bcc(100), bcc(110) and bcc(111), have been implanted into the middle of the simulation box. Except the fcc(111) template, whose structure benefits not only fcc but also hcp crystals resulting in a similar behavior to homogeneous crystallization, bcc-type templates favor the formation of bcc crystals and bcc-like precursors while fcc-type templates favor the formation of fcc crystals and fcc-like precursors. Therefore, for fcc(100) and fcc(110) templates, heterogeneous crystallization will definitely result in a fcc crystallite. However, the results of heterogeneous crystallization that are induced by bcc-type templates are subtly different at different state points. At the state points where the interaction strength of charged colloids is weak and the fcc phase is thermodynamically stable, the bcc crystals formed with the promotion of bcc-type templates are not stable so as to tend to transform into fcc or hcp crystals. When the interaction strength of charged colloids is high, the predominant bcc crystals formed with the promotion of bcc-type templates can always persist within the time scale of simulation although not bcc but fcc crystals are thermodynamically stable.

1. Introduction

Colloids, whose typical sizes range from a few nm to several μm, are often used as a valuable model system to study a lot of phenomena happening in physics, chemistry, materials science, biology and other fields since they allow us to experimentally observe the dynamic process of various phase behaviors at a single-particle level.[1–4] Among those research studies, an important one is to employ a colloidal system to study the crystallization process so as to generally reveal the underlying mechanism.[5,6] In addition to the scientific significance, the crystals obtained from the colloidal system are excellent materials which have been greatly applied to many fields such as micro- and nano-optical devices, color printing, sensors, bionic materials, energy conversion and storage materials, and biomedicine.[7–13]

There are already a great number of ways to produce colloidal crystals. A simple and natural approach is to prepare suitable colloidal suspensions and just wait for the disorder–order phase transition to happen under appropriate conditions.[9,11,12] Such a "let it go" strategy, which is also regarded as a bottom-up route, may obtain the desired product, but unfortunately the crystal quality is not controllable and the production efficiency is probably unsatisfactory. Afterwards some external fields such as electric and magnetic fields, gravity, flat or structured substrates, and shear have been suggested to be exerted during colloidal crystallization in order to improve the fabrication efficiency and quality of colloidal crystals.[9,12,14] The template-assisted method is a very popular fabrication technique because the implanting of a structured interface does not change the physical and chemical properties of colloidal particles but meanwhile can influence the crystallization process significantly by simply modifying the patterns of the substrate. Long ago, it was already found that the quality of colloidal crystals can be greatly improved with the help of a suitable template.[15] Moreover, by changing the morphology, structure and other properties of the template interface, the nucleation pathway and crystallization procedure can possibly be regulated, so as to finally affect the obtained crystal structures.[16–22]

In recent decades, template-induced crystallization has been studied extensively for a simple model colloidal system, *i.e.* hard-sphere colloids.[23–30] Even for a flat smooth substrate which has no lateral structure, there always exist wetting

[a] *Key Laboratory of Microgravity, Institute of Mechanics, Chinese Academy of Sciences, Beijing 100190, China. E-mail: oywz@imech.ac.cn, xush@imech.ac.cn; Fax: +86 1082544096; Tel: +86 1082544099*
[b] *College of Materials Engineering, North China Institute of Aerospace Engineering, Langfang 065000, China*
[c] *School of Engineering Science, University of Chinese Academy of Sciences, Beijing 100049, China*

behaviour and pre-crystallization transition in the bulk fluid of hard spheres.[24,25] Auer and Frenkel showed that flat hard walls can decrease the free energy barrier to about two orders of magnitude compared with bulk hard spheres.[23] They also found that the first layer of hard-sphere particles that crystallize on a smooth hard wall has the structure of the fcc(111) plane and the final formed crystal is a mixture of fcc and hcp structures. For patterned substrates in hard spheres, it has been found that the structures of the substrate surface play a crucial role in the kinetics of crystallization and the resulting crystal structures.[26,27,30] However, the actual interaction between many kinds of colloids is not so simple as hard spheres and the corresponding liquid–solid phase transition is often complex indeed. Here we will consider the template-induced crystallization of charged colloids,[31] as the interaction between charged colloidal particles can be tuned in a fairly large range by changing some parameters (such as particle size, volume fraction, particle's surface charge, and ion concentration in solution), which can correspond to various kinds of systems (*e.g.*, when the particle's surface charge is extremely weak, it can degenerate into a simple hard-sphere colloid) and make the obtained results have strong universality to help us understand the general crystallization mechanism.[6]

In physics, template-induced crystallization is a kind of heterogeneous crystallization. Unlike homogeneous crystallization that happens in bulk fluids, the substrate surface is expected to play an important role in crystal nucleation and subsequent crystal growth.[16–22] So far, homogeneous crystallization in charged colloids has already been studied in detail and the underlying mechanism is understood well. Many previous studies have proved that homogeneous crystallization is often not completed in one step as described by the classical nucleation theory (CNT), but is carried out in two or even many steps.[32–36] Not only is the relatively ordered precursor (liquid phase with a high orientational order) formed before crystal nucleation, but also some metastable crystal structures (metastable bcc or hcp) may show up and even always exist with the thermodynamically stable structure resulting in a polycrystal finally. To the best of our knowledge, heterogeneous crystallization in charged colloids, specifically crystallization on different patterned templates, has not been systematically studied yet.[21,37,38] By using charged colloids as a model system, we wish to answer some questions relevant to heterogeneous crystallization on structured substrates: Which kind of structured substrates can lead to the formation of a desired single crystal that is used as a functional material? What are the requirements or the optimization conditions for the preparation of high-quality single crystals with few defects? Particularly, we will make an effort to completely understand the underlying mechanism of template-induced crystallization. By addressing these issues mentioned above, we expect to explore the law of heterogeneous crystallization on patterned substrates so as to provide suitable conditions for the efficient fabrication of high-quality colloidal crystals that satisfy actual requirements in functional applications. From a scientific point of view, we believe this will shed new insight into the physics of heterogeneous crystallization.

In this article, we plan to perform brute-force molecular dynamics (MD) simulations which are straightforward and can directly provide a "real" temporal evolution to study the template-induced crystallization process of charged colloids at a microscopic level. The number of colloidal particles we use is more than 10^5 which is large enough so that not only the stage of crystal nucleation but also the stage of crystal growth can be investigated. In order to accelerate MD simulations, we implement a graphics processing unit (GPU)-accelerated parallel algorithm[39,40] on the platform of compute unified device architecture (CUDA).[41] As the liquid–solid phase diagram of charged colloids has both bcc and fcc phase regions, here we use different templates whose structures are compatible with the bcc or fcc phase, *i.e.*, they are in practice some typical planes of bcc or fcc crystals. By inserting patterned templates, we systematically study the effect of different templates on the heterogeneous crystallization of charged colloids. Our investigation focuses on the kinetic process of heterogeneous crystallization and also the obtained crystal structures to compare with the results of homogeneous crystallization in bulk charged colloids.

2. Models and simulation methodology

According to the theory of Derjaguin, Landau, Verwey, and Overbeek (DLVO),[42] a repulsive Yukawa potential can be used to mimic the electrostatic interaction between charged colloidal particles, which is written by

$$U_{\mathrm{Yukawa}}(r) = \varepsilon\frac{\exp[-\kappa(r/\sigma-1)]}{r/\sigma}, \quad (1)$$

The excluded volume of colloids is modeled by a Weeks–Chandler–Anderson (WCA) potential

$$U_{\mathrm{WCA}}(r) = \begin{cases} 4\varepsilon_{\mathrm{W}}\left[(\sigma/r)^{12}-(\sigma/r)^{6}+\frac{1}{4}\right], & r < 2^{1/6}\sigma \\ 0, & \text{else} \end{cases}. \quad (2)$$

So the full interaction between colloids is the summation of the Yukawa and WCA potential, *i.e.*, $U(r) = U_{\mathrm{WCA}}(r) + U_{\mathrm{Yukawa}}(r)$.[33,35] σ is the diameter of charged colloids, and κ is the inverse screening length referring to the electrostatic interaction. The parameters ε and ε_{W} govern the strength of repulsive Yukawa potential and WCA potential, respectively. In reduced units that are often used in computer simulations, we define $\sigma = 1$ and $\varepsilon_{\mathrm{W}} = k_{\mathrm{B}}T = 1$ where k_{B} is the Boltzmann constant and T is the desired temperature of the colloidal system.

In this work, we consider a set of templates, *i.e.*, the patterned substrates including (100), (110), and (111) planes of both bcc and fcc crystals, as shown in Fig. 1. Such structures of templates are expected to be commensurate with the bulk crystals of charged colloids based on the constructed phase diagram.[43] The MD simulations are performed in a cubic box, where the period boundary conditions are applied. The plane of the structured template is perpendicular to the Z axis and

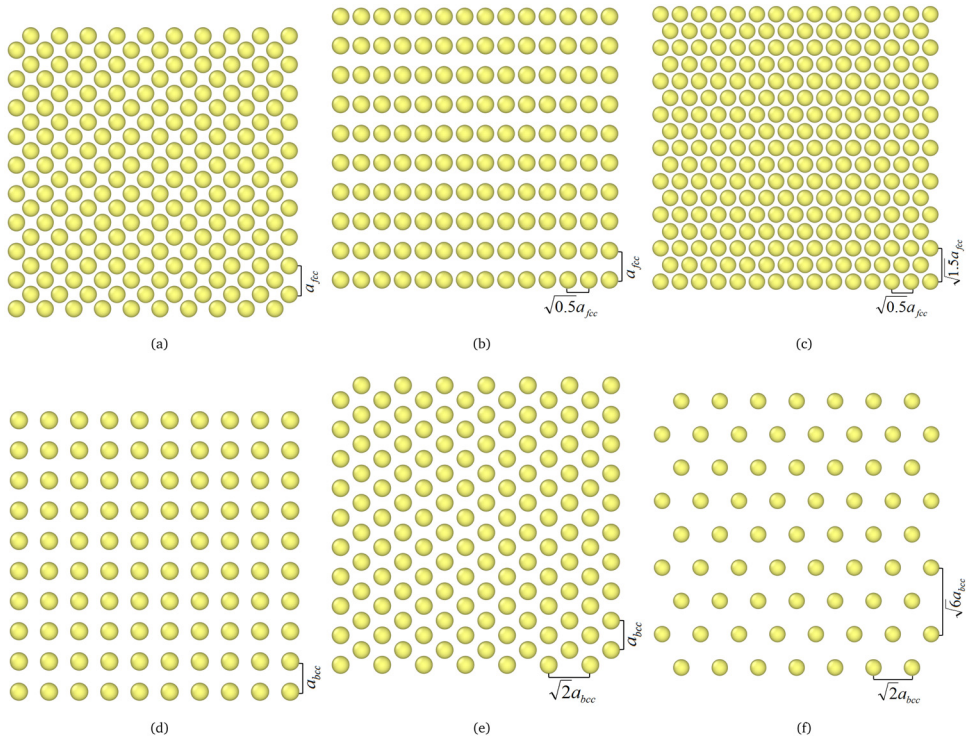

Fig. 1 Different structured templates used in the MD simulation, which are in the x–y plane of the simulation box and formed by a periodic array of fixed charged colloids. (a) The fcc(100) template; (b) fcc(110) template; (c) fcc(111) template; (d) bcc(100) template; (e) bcc(110) template; (f) bcc(111) template. a_{fcc} and a_{bcc} are the lattice length of fcc-type and bcc-type templates whose areas are adjusted to the equilibrium solid density at the state point of interest, *i.e.*, $a_{\mathrm{fcc}} = \sqrt[3]{4/\rho}$ and $a_{\mathrm{bcc}} = \sqrt[3]{2/\rho}$.

inserted in the middle of simulation box, which is similar to what had been done in ref. 27. The ensemble we use is *NVT*, *i.e.* the number of total particles (including the particles on the template), the length of simulation box, and the temperature are kept fixed during each MD simulation. Notice here that the particles on the template do not move at all and their number is commensurate with the structures of the template, which is also corresponding to the length of the simulation box, as summarized in Table 1. After the particles on the template are set, the bulk particles that can move are initially put into the simulation box with a random distribution for the positions and a Maxwellian distribution for the velocities. The equation of particle's motion is integrated *via* the velocity-Verlet algorithm. To control the desired temperature, we adopt the Berendsen thermostat.[44]

During a typical crystallization event, we should know the ordering of particles that happens simultaneously. Here we mainly concentrate on a rotational ordering that is related to the bond-orientational order (BOO) parameters.[45] To avoid the misleading in the calculation of BOO parameters,[46,47] we first of all construct the Voronoi diagram for an appropriate assignment of nearest-neighbor particles. For a particle i, its Voronoi cell has several facets which separates it from a few nearest-neighbor particles. Assuming that a nearest-neighbor particle is j and the corresponding surface area of the Voronoi cell facet is A_{ij}, the total surface area would be $A_{\mathrm{tot}}(i) = \sum_{j=1}^{N_{\mathrm{nb}}(i)} A_{ij}$, where N_{nb}

Table 1 Details of the simulation box, crystal growth rate and growth interface for different pattered templates (see Fig. 1) at two typical state points. In the MD simulation, the fixed inverse screening length is $\kappa = 5.0$ and the total number of particles (including N_{temp} colloidal particles on the template) used is $N = 131\,072$. The thermodynamically stable phase is fcc referring to the phase diagram constructed previously (see Fig. 2). The crystal growth rate v_{g} is estimated by fitting linearly the curve of solid surface height *versus* time (see the middle of Fig. 5). Here we only give the results of the growth interface at a typical crystal growth time $t = 10^4\delta t$. The interface thickness l_{T} is obtained *via* the fitting of the Q_6 profile along the z axis (see eqn (9) and the bottom of Fig. 5). The interface roughness l_{R} is calculated by the total Voronoi volume of precursors on the interface divided by the area of the x–y plane. The last digits in parentheses indicate the statistical errors

Template	N_{temp}	L_x	L_y	L_z	v_g	l_{T}	l_{R}
$\varepsilon = 2$, $\rho = 1.0$							
bcc(100)	1024	40.317	40.317	80.635	0.438(8)	2.08	4.35
bcc(110)	2048	57.018	40.318	57.018	0.366(11)	1.85	3.53
bcc(111)	1024	49.379	57.018	46.555	0.366(12)	2.09	3.9
fcc(100)	2048	50.797	50.797	50.797	0.574(7)	1.8	2.1
fcc(110)	1024	35.919	50.797	71.838	0.393(7)	1.52	2.38
fcc(111)	2048	35.919	62.213	58.655	0.286(7)	2.44	4.01
$\varepsilon = 20$, $\rho = 0.55$							
bcc(100)	1024	49.208	49.208	98.417	0.716(8)	2.42	4.18
bcc(110)	2048	69.591	49.208	69.591	0.659(9)	2.4	3.75
bcc(111)	1024	60.268	69.591	56.821	0.573(14)	2.13	4.18
fcc(100)	2048	61.999	61.999	61.999	0.576(10)	2.91	3.08
fcc(110)	1024	43.84	61.999	87.679	0.393(8)	2.14	3.21
fcc(111)	2048	43.84	75.933	71.59	0.398(14)	3.52	4.94

is the total number of nearest-neighbors of particles i. Then a complex vector $q_{lm}(i)$ for the particle i is defined as

$$q_{\mathrm{lm}}(i) = \frac{1}{N_{\mathrm{nb}}(i)} \sum_{j=1}^{N_{\mathrm{nb}}(i)} \frac{A_{ij}}{A_{\mathrm{tot}}(i)} Y_{lm}(\mathbf{r}_{ij}). \quad (3)$$

Here $\mathbf{r}_{ij}$ is the vector from particle i to j and $Y_{\mathrm{lm}}(\boldsymbol{r}_{ij})$ is its spherical harmonics function.[48] l is a free integer parameter and m is an integer that runs from $m = -l$ to $m = l$.

To identify crystal particles, Frenkel and coworkers[49,50] proposed a method which has become very polar in the study of crystal nucleation. In this method, l is taken as $l = 6$ and the complex vector $q_{6m}(i)$ is normalized to $d_{6m}(i)$

$$d_{6m}(i) = \frac{q_{6m}(i)}{\left[\sum_{m=-6}^{6} |q_{6m}(i)|^2\right]^{1/2}}. \quad (4)$$

Then a scalar product is calculated to measure the correlation between neighboring particles i and j

$$S_{ij} = \sum_{m=-6}^{6} d_{6m}(i) \cdot d_{6m}^{*}(j), \quad (5)$$

where the superscript * indicates complex conjugation. If S_{ij} exceeds a threshold value (here we set it arbitrarily as 0.7), these two neighboring particles i and j are connected. When a particle has at least 7 connected neighbors, we say it is a solid or crystal particle.

To further determine the crystal structure, we use the coarse-grained method introduced by Lechner and Dellago.[51] First, we average q_{lm} over all the nearest neighbours of particle i and particle i itself to get

$$\bar{q}_{lm}(i) = \frac{1}{N_{\mathrm{nb}}(i)} \sum_{k=0}^{N_{\mathrm{nb}}(i)} q_{lm}(k), \quad (6)$$

where $k = 0$ means particle i itself. Then we can calculate two local BOO parameters

$$Q_l(i) = \left(\frac{4\pi}{2l+1} \sum_{m=-l}^{l} |\bar{q}_{lm}(i)|^2\right)^{1/2}, \quad (7)$$

and

$$W_l(i) = \sum_{m_1+m_2+m_3=0} \begin{pmatrix} l & l & l \\ m_1 & m_2 & m_3 \end{pmatrix} \frac{\bar{q}_{lm_1}(i)\bar{q}_{lm_2}(i)\bar{q}_{lm_3}(i)}{\left(\sum_{m=-l}^{l} |\bar{q}_{lm}(i)|^2\right)^{3/2}}, \quad (8)$$

where the term in parentheses is the Wigner $3-j$ symbol. The integers m_1, m_2, and m_3 run from $-l$ to l with the precondition that $m_1 + m_2 + m_3 = 0$. Similar to the precursor-mediated scenario existing in homogeneous crystallization, here we define the precursor particles by using a threshold value of Q_6 (typically liquid particles with $Q_6 \geq 0.25$). From the sign of W_6 and W_4,[52] we can know the local symmetry of a particle i: (i) fcc type as $W_6(i) < 0$ and $W_4(i) \leq 0$; (ii) hexagonal close-packed (hcp) type as $W_6(i) < 0$ and $W_4(i) > 0$; (iii) bcc type as $W_6(i) \geq 0$.

3. Results and discussion

In this work, six kinds of structured templates have been considered (see Fig. 1). The box lengths of x and y directions are adjusted to fulfill the structure of the template while the box length of the z direction is extended to investigate the crystal growth conveniently, all of which are listed in Table 1. The total number of particles (including the particles on the template) we take is $4 \times 32^3 = 131\,072$. In the constructed phase diagram of charged colloids (see Fig. 2), the region of the bcc phase is very narrow and mostly the stable phase should be fcc. However, our previous studies have shown that the metastable bcc phase probably appears first and even remains for a rather long time[32,35] in some regions of the fcc phase, which is considered to be a manifest of Ostwald's step rule. Here we keep $\kappa = 5.0$ fixed and mainly choose two typical points for both low interaction strength and higher interaction strength in the fcc phase region, *i.e.*, $\varepsilon = 2$, $\rho = 1.0$ and $\varepsilon = 20$, $\rho = 0.55$ (see the crosses shown in Fig. 2), where the degree of supercooling in units of melting temperature T_{m} is approximately $0.75T_{\mathrm{m}}$ and $0.78T_{\mathrm{m}}$ respectively. Assuming $\Delta\mu = \Delta h_{\mathrm{m}}(1 - T/T_{\mathrm{m}})$ where Δh_{m} is the enthalpy of fusion per particles at the melting temperature, we can estimate the difference in chemical potential between the liquid and the crystal phase, *i.e.*, $\Delta\mu = 1.29$ for $\varepsilon = 2$, $\rho = 1.0$ and $\Delta\mu = 0.61$ for $\varepsilon = 20$, $\rho = 0.55$. Notice that we have in advance performed simulations at these two state points without templates to ensure that the homogeneous crystallization does not happen up to $t = 10^7\delta t$ (see the results shown in Table 2).

3.1 The layering crystallization and growth rate

As shown in Fig. 3, we plot a few snapshots during a typical heterogeneous crystallization process (the template is fcc(100) and the state point is $\varepsilon = 2$, $\rho = 1.0$). In order for a further view of the crystallization process, we also calculate the density profiles along the z-direction at varying simulation time which are

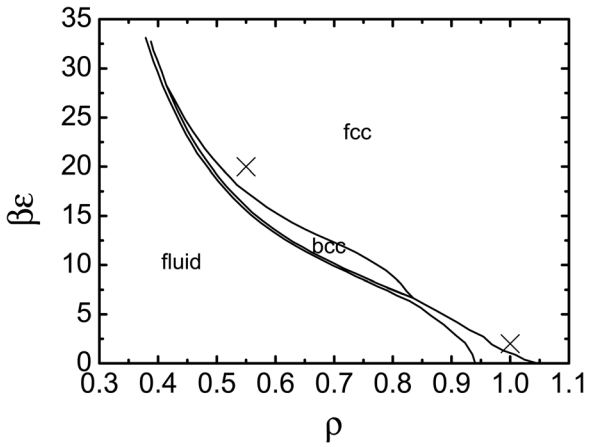

Fig. 2 Phase diagram of charged colloids, which is reproduced from the data in ref. 43. The effective interaction between charged colloids is modeled by a hard-core Yukawa potential (see eqn (1) and (2)), where $\beta = k_{\mathrm{B}}T = 1.0$ and the inverse screening length $\kappa = 5.0$. The crosses show the state points ($\varepsilon = 2$, $\rho = 1.0$ and $\varepsilon = 20$, $\rho = 0.55$) concerned in this work.

Table 2 Fractional compositions of both crystals and precursors in MD simulations of bulk charged colloids without templates. The state points of charged colloids considered here is $\varepsilon = 2$, $\rho = 1.0$ and $\varepsilon = 20$, $\rho = 0.55$ while the inverse screening length is fixed as $\kappa = 5.0$. The bulk charged colloids at these two state points are always trapped into a metastable stage where many small nuclei form and dissolve but cannot grow up to a critical size. When calculating the fractional compositions, we include all of the crystal or precursor particles in the whole system together

	Fractional crystals			Fractional precursors		
State point	f_{fcc}	f_{hcp}	f_{bcc}	$f_{fcc\text{-}like}$	$f_{hcp\text{-}like}$	$f_{bcc\text{-}like}$
$\varepsilon = 2$, $\rho = 1.0$	0.378	0.241	0.381	0.221	0.280	0.499
$\varepsilon = 20$, $\rho = 0.55$	0.302	0.218	0.480	0.191	0.258	0.551

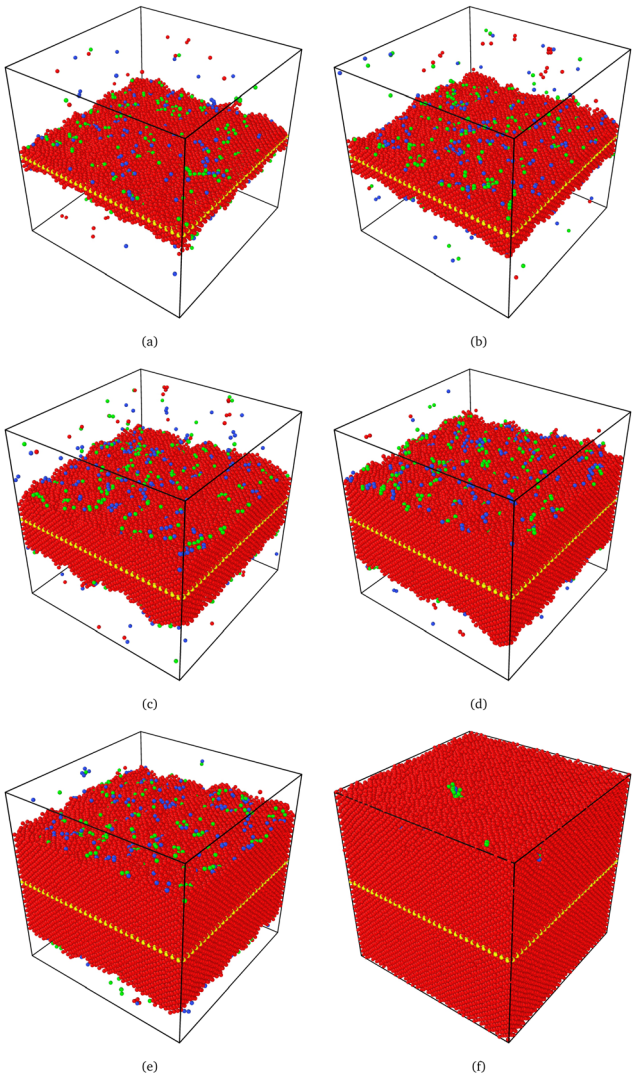

Fig. 3 Snapshots during a typical heterogeneous crystallization process which is induced by the fcc(100) template at the state point $\varepsilon = 2$, $\rho = 1.0$. Red, green, blue, and yellow spheres represent fcc, hcp, bcc and template particles, respectively. Liquid particles are not plotted in order for a clear view. (a) $t = 10^3\delta t$. (b) $t = 2 \times 10^3\delta t$. (c) $t = 5 \times 10^3\delta t$. (d) $t = 8 \times 10^3\delta t$. (e) $t = 10^4\delta t$. (f) $t = 5 \times 10^4\delta t$.

corresponding to the plotted snapshots (see Fig. 4). In agreement with previous investigations,[19,21,23,26,27,29] the heterogeneous

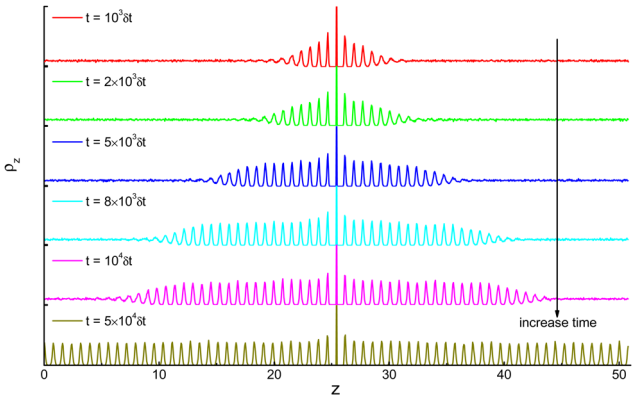

Fig. 4 Density profiles along the z-direction corresponding to Fig. 3. The profiles are accumulated by the way that the box length of the z-direction (see Table 1) is divided into 1000 bins. From the top to bottom, the time (see the inside of the panels) is increased from $t = 10^3\delta t$ to $t = 5 \times 10^4\delta t$.

crystallization happens very soon indicating that the implanting of the template does promote the crystallization significantly. Clearly shown in the snapshots and density profiles, the colloidal crystals grow layer by layer with the proceeding of heterogeneous crystallization. Even at the very beginning of crystallization, a few crystalline layers near the substrate have already formed. With the growth of crystal layers, most of the colloidal particles in the system will become solid finally although there are some subtle differences for different templates and state points (see the following parts of this paper). Notice here that there will be some density variations for crystals and liquids when crystallization proceeds. We have calculated the densities of both liquids and crystals (see the top of Fig. 5) and find that the difference between disordered liquid density and starting density is always less than 5%. For $\varepsilon = 20$, the difference between liquid density and starting density is even less than 2%), which will not bring the fluid to the bcc stability region (at the bcc boundary, $\rho \approx 0.5$).

It is interesting to calculate the crystal growth rate of the heterogeneous crystallization which is in principle related to the fabrication efficiency of colloidal crystals. From the definition, the crystal growth rate is exactly the growth velocity of the liquid–solid interface. Here we can observe the growth of layering crystals during the heterogeneous crystallization process (see Fig. 3 and 4) and get the temporal evolution of the crystal's height which approximately shows a linear curve. Then by doing a linear fit for the curve of crystal height *versus* time we measure the crystal growth rate (see Fig. 5). In practice, the crystal surface is not strictly a perfect plane so we must calculate an effective crystal height. Assuming that all the layering crystals in the simulation box grow along the direction of z axis, the effective crystal height can be obtained by the division between the occupied volume of growing crystal cluster and the area of x–y or template plane. The volume of the crystals can be evaluated by the summation of each Voronoi cell's volume occupied by the solid particles in the growing crystal cluster. In Table 1, we show the crystal growth rate of heterogeneous crystallization induced by different pattered templates for each state point. Notice here that each crystal

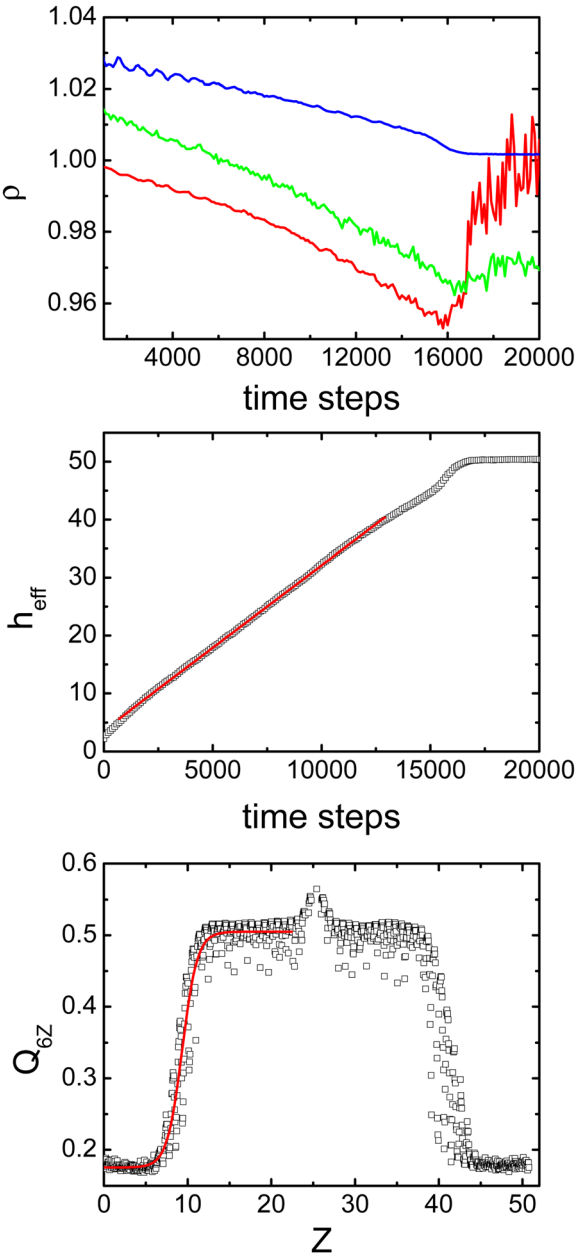

Fig. 5 Crystal growth and interface BOO profile during a typical heterogeneous crystallization induced by fcc(100) template at the state point $\varepsilon = 2$, $\rho = 1.0$, corresponding to Fig. 3. Top: Evolution of the average density of various structures. For each particle, its local density can be exactly calculated *via* the occupied volume of the corresponding Voronoi cell. Red, green and blue lines represent the average density of crystals (excluding crystals on the template), precursors and disordered liquids (liquids with $Q_6 < 0.25$) respectively. Middle: Evolution of the effective crystal height h_{eff}. The effective crystal height is calculated by the division between the volume of growing crystallite and the area of the template plane. Squares represent the data of h_{eff} while the red line represents the linear fit to temporal h_{eff}. After counting all the growth rates of fifty MD samples of heterogeneous crystallization, we can obtain the averaged growth rate as is shown in Table 1. Bottom: The profile of the BOO parameter Q_6 along the z axis at $t = 10^4\delta t$. Squares represent the data of the Q_6 profile while the red line shows the fitting curve (only fitting the left side of the interface as the two sides are approximately symmetrical) by eqn (9).

growth rate listed in Table 1 is obtained by averaging over fifty MD samples for satisfying statistics. The crystal growth rate of the bcc(100) template is largest among all the results of bcc-type templates, while the crystal growth rate of the fcc(100) template is largest among all the results of fcc-type templates. At weak interaction strength ($\varepsilon = 2$, $\rho = 1.0$) where bcc crystals are likely unstable and tend to transform into fcc or hcp crystals (see Section 3.2), the crystal growth rate of the fcc(100) template is largest among all the heterogeneous crystallization events. At higher interaction strength ($\varepsilon = 20$, $\rho = 0.55$) where metastable bcc crystals are difficult to transform into fcc or hcp crystals (see Section 3.3), the crystal growth rates of bcc-type templates are often fairly high so that the bcc(100) template should result in the largest crystal growth rate.

3.2 At low interaction strength ($\varepsilon = 2$, $\rho = 1.0$)

At low interaction strength when the interactions between charged colloids are weak, the particles of charged colloids behaves like hard spheres. As has been studied extensively,[33,35] the stable phase is fcc and the metastable bcc phase is minor during the whole crystallization process although there are some other subtle details compared with the hard-sphere system.

As the template with fcc symmetry is commensurate with the bulk crystal, it can be expected that the formation of fcc crystal is favored. Fig. 6 shows the fraction of different crystal structure evolves with the time steps during a typical crystallization process with the induction of fcc(100), fcc(110) and fcc(111) templates, respectively. For fcc(100) and fcc(110) templates, the crystals formed are mostly fcc and only very few bcc crystal particles are attached on the surface of crystallites during crystallization. For the fcc(111) template, the case is different because the fcc(111) plane benefits not only the formation of fcc but also the formation of hcp.[26] Actually the crystallization induced by the fcc(111) plane leads to a mixture of fcc, hcp and bcc structures (see Fig. 6(c)), which is rather similar to the homogeneous crystallization of charged colloids.[33–35]

When implanting the template with bcc symmetry, the crystallization process and resulting crystal structures become complicated. As the thermodynamically stable phase at $\varepsilon = 2$, $\rho = 1.0$ is fcc and bcc phase is not stable at all, the formed bcc crystals induced by the template may probably tend to transform into fcc or hcp crystals. Although the bcc-type template should in common make the crystal nucleation of bcc structure easier, the effect of induction to the crystallization, with respect to the template of different bcc planes, has a subtle difference in fact. For bcc(100) and bcc(111) templates, the crystals formed at first are mostly bcc structures, and then the bcc crystallite grows to almost expand the whole simulation box. But the bcc crystals are so unstable that many of them slowly transform into fcc or hcp crystals eventually. For bcc(110), there are only a few layers of bcc crystals formed before they begin to transform into fcc or hcp crystals suggesting that the bcc crystals induced by bcc(110) are more likely to be unstable. For all the bcc-type templates, the final crystal structures obtained are a mixture of bcc, fcc and hcp (see Fig. 6). In particular, the early formed bcc

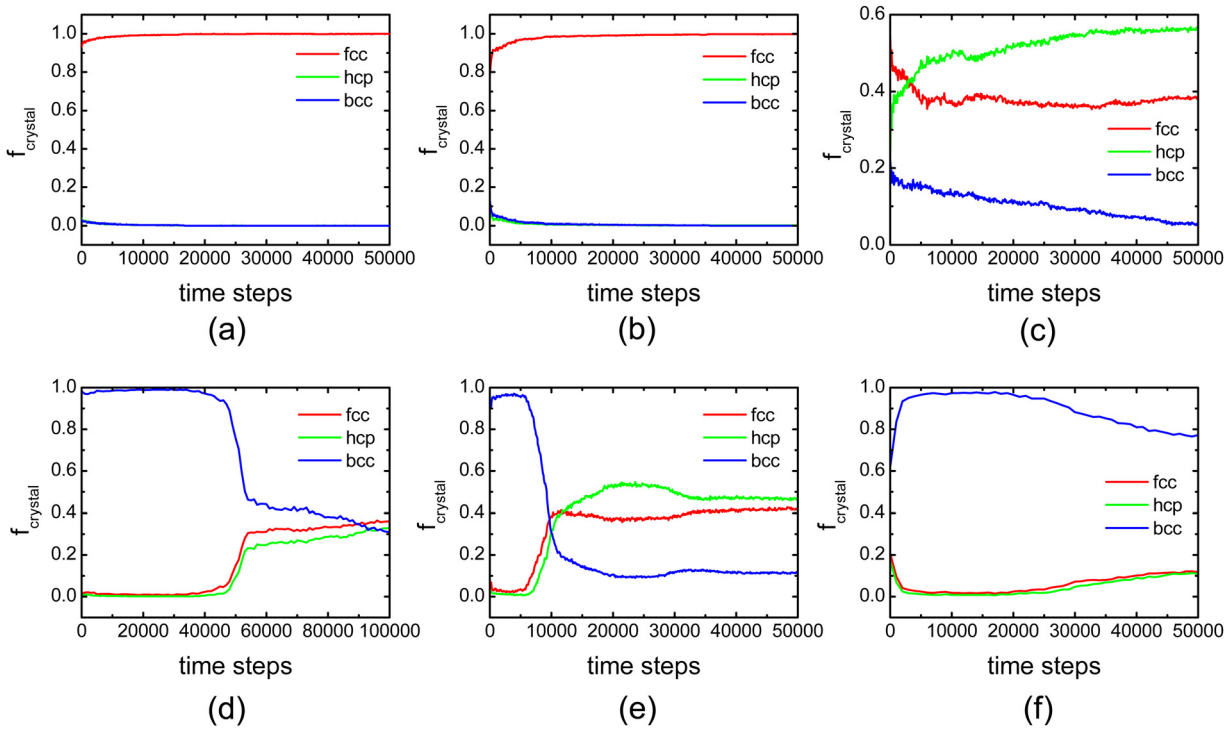

Fig. 6 Temporal fraction of each polymorph during a typical heterogeneous crystallization process assisted by different structured templates when $\varepsilon = 2$, $\rho = 1.0$. (a) fcc(100) template. (b) fcc(110) template. (c) fcc(111) template. (d) bcc(100) template. (e) bcc(110) template. (f) bcc(111) template. Red, green and blue lines represent fcc, hcp, and bcc polymorphs, respectively.

crystals near the bcc-type template will even remain for a very long time when the crystallization proceeds further, as if the template can prohibit the bcc crystals nearby from transforming into fcc or hcp crystals. These results are reminiscent of the hard-sphere crystallization induced by a bcc(100) template,[27] in which the bcc crystals far away from the bcc(100) template can also transform into fcc or hcp crystals eventually while the ordered hard-sphere particles near the template have bcc symmetry because they inherit the character of a patterned template.

3.3 At higher interaction strength ($\varepsilon = 20$, $\rho = 0.55$)

According to the Ostwald's step rule[53] and Alexander-McTague mechanism[54] which was first proposed in homogeneous crystallization, the bcc crystal should be favored despite the fcc phase being the most stable especially when a weak first-order phase transition happens. Specifically in the homogeneous crystallization of charged colloids, the formation of predominant metastable bcc crystal has been investigated both in experiments and computer simulations[32,33,35] when the interaction strength is high and the state point is near the liquid–solid line where the supersaturation is high enough to make the liquid–solid phase transition weak. At the state point $\varepsilon = 20$ and $\rho = 0.55$), we have performed MD simulations of bulk liquid and do not see the crystal nucleation for an extremely long time, which indeed verifies a high enough supersaturation. Concerning the heterogenous crystallization, it is interesting to ask a question such as what will happen when implanting a patterned template with bcc or fcc symmetry.

We first study the heterogeneous crystallization with the template of fcc symmetry. As is shown in Fig. 7, the results of both fcc(100) and fcc(110) templates are similar to those of low interaction strength (see Fig. 6), *i.e.*, most of crystals formed during the whole crystallization process are fcc while the bcc crystal is a tiny minority. As for the heterogeneous crystallization of the fcc(111) template, it leads to a mixture of fcc, hcp and bcc crystals as expected. But the fraction of bcc crystal, in the late stage of crystallization, becomes dominant over fcc and hcp crystals again which is also found in homogeneous crystallization of charged colloids.[35]

Since it is already discovered in the study of homogenous crystallization where there is no template involved that a bcc predominant crystalline is achieved, we expect the formation of bcc crystals will be promoted even more when inserting a bcc-type template into charged colloids. As can be seen from Fig. 7, for all the bcc type template the resulting crystallites have the structure of dominant bcc ordering and there are very few fcc and hcp crystals inside. This is not surprising considering the results of predominant bcc crystals formed in homogeneous crystallization of charged colloids. However, we should notice here that the thermodynamically stable phase is fcc but not bcc. From the thermodynamics point of view, the obtained bcc will somehow transform into stable fcc sooner or later. But here the free-energy barrier of bcc–fcc transition is too high to be overcome easily so as to make the lifetime of metastable bcc much longer than the time scale of simulation. Indeed such a long-lived metastable bcc phase has been observed frequently in previous numerical studies.[32,33,35]

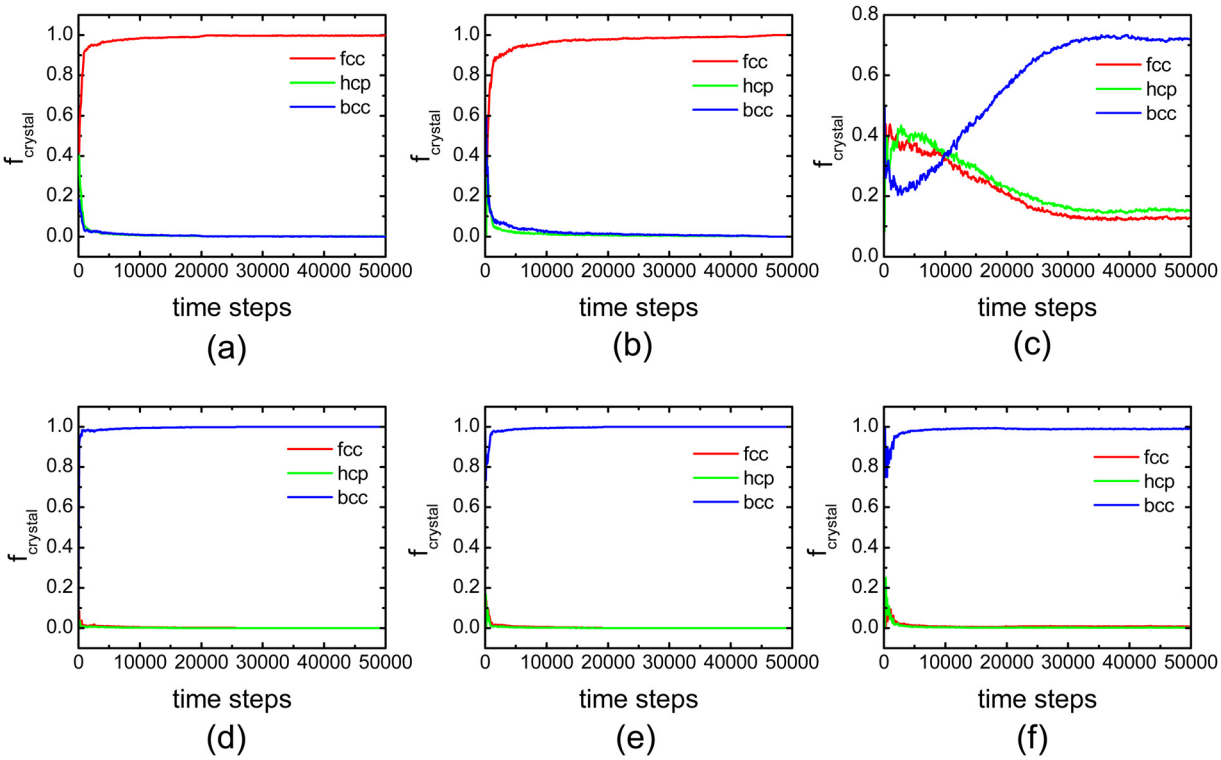

Fig. 7 Temporal fraction of each polymorph during a typical heterogeneous crystallization process assisted by different structured templates when $\varepsilon = 20$, $\rho = 0.55$. (a) fcc(100) template. (b) fcc(110) template. (c) fcc(111) template. (d) bcc(100) template. (e) bcc(110) template. (f) bcc(111) template. Red, green and blue lines represent fcc, hcp, and bcc polymorphs, respectively.

3.4 The mediated precursor

The relatively ordering precursor, as a mediated structure that is different from the one-step picture described in CNT, has been observed and proved to be nontrivial in both homogeneous and heterogeneous crystallization.[19,21,33–36,45,52] Generally speaking, a liquid particle will not directly transform into a solid in one step when a crystallization event happens. Instead, it will firstly become relatively ordered but still does not run into a solid state. Such a relatively ordered particle is named as a precursor particle. As the local order parameter Q_6 (see eqn (7)) that exactly indicates the degree of a particle's ordering has been suggested to be the crucial factor that drives the crystal nucleation (see Fig. 8),[45] we identify a particle as the precursor particle when its local order parameter Q_6 is larger than a threshold value (here we arbitrarily take it as 0.25) but its connected neighbors is less than 7 (which means the particle is still a liquid particle). The symmetry type of a precursor particle is decided by the sign of order parameters W_4 and W_6. For precursors, here we consider three types of structures based on their symmetries, *i.e*, fcc-like, hcp-like and bcc-like precursors, similar to the identification of crystal structure. More details for the identification method related to order parameters can be found in Section 2.

In MD simulations of homogeneous crystallization without templates, the colloidal systems we consider in this work are always trapped into a metastable stage where many small nuclei form and dissolve but cannot grow up to a critical size.

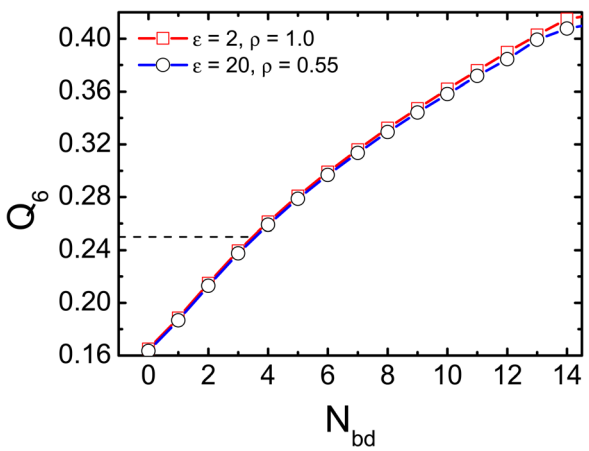

Fig. 8 The local order parameter Q_6 as a function of the connected neighbors (see eqn (5)). The data are obtained during MD simulations (without templates) at the two considered state points $\varepsilon = 2$, $\rho = 1.0$ and $\varepsilon = 20$, $\rho = 0.55$. The dashed line indicates the threshold value (here is 0.25) used in this work to identify precursor particles. Notice here that the threshold value of connected neighbors to determine a solid particle is 7, corresponding to $Q_6 \approx 0.315$.

As is listed in Table 2, we calculate the fractional compositions of precursors appearing in the whole system in order for a comparison with heterogeneous crystallization. In the template-induced heterogenous crystallization, the precursor particles that will subsequently become solid and join in the crystallite are mostly

attached on the moving liquid–solid surface. We observe the influence of both fcc-type and bcc-type templates on the precursor formation during heterogeneous crystallization. When using the fcc(111) template, it seems to promote the formation of fcc precursors very little as if it leads to results similar to those of homogeneous crystallization (see also the crystal structures stated in Sections 3.2 and 3.3). In contrast, fcc(100) and fcc(110) templates can promote the formation of fcc-like precursors (see Fig. 9 and 10) whereas bcc-like precursors are still dominant during the growth of layering crystals. As for the crystallization induced by the bcc-type templates, we find that the bcc-type templates significantly promote the formation of bcc-like precursors especially at the early stage of crystallization (see Fig. 9 and 10). When the crystallite grows layer by layer, the template is buried by the newly formed crystals suggesting that not the bcc crystal particles on the template but the crystal particles on the liquid–solid surface influence the subsequent formation of precursors. For the cases where the long-lived metastable bcc crystals are induced by the bcc-type templates to form first, the crystals on the liquid–solid surface are always predominant bcc so that the fractions of attached bcc-like precursors is much larger than that of homogeneous crystallization (see Fig. 9(d) and (f)).[35] However, when the lifetime of bcc crystals are short, the evolution of fractional precursors is different. As shown in Fig. 6(e) (the crystallization with bcc(110) template at $\varepsilon = 2$ and $\rho = 1.0$), the bcc crystals are so unstable that they soon begin to transform into fcc or hcp crystals after a few layers of bcc crystals form. As a result, the fraction of bcc-like precursors is at first very large but then decreases (see Fig. 9(e)).

With the physics picture of crystal growth, we can further understand and explain the results of crystal growth rate (see Section 3.1). Here we examine several profiles of the growth interface, *i.e.*, the BOO parameter, the thickness and the roughness of interface, which have been found highly related to the crystal growth rate.[55–57] First, we calculate the profile of Q_6 along the z axis and then use the following form to fit the data of Q_{6Z} (see the bottom of Fig. 5)

$$Q_{6Z}(z) = \frac{Q_S + Q_L}{2} + \frac{Q_S - Q_L}{2}\tanh[(z - z_0)/l_T], \qquad (9)$$

where l_T is a measure of the interface thickness, while Q_S and Q_L are the bulk Q_6 of solid and liquid phase respectively. We define the roughness of the interface as the total occupied Voronoi volume of pre-ordered precursor particles on the interface divided by the area of x–y plane. We chose a typical time of crystal growth, *i.e.*, $t = 10^4\delta t$, to estimate the interface thickness and roughness, as listed in Table 1. For fcc-type templates, both the interface thickness and roughness of the fcc(111) template are larger than those of fcc(100) and fcc(110) templates, which can explain why the crystal growth rate of fcc(111) is not large. Comparing the fcc(100) template with the fcc(110) template,

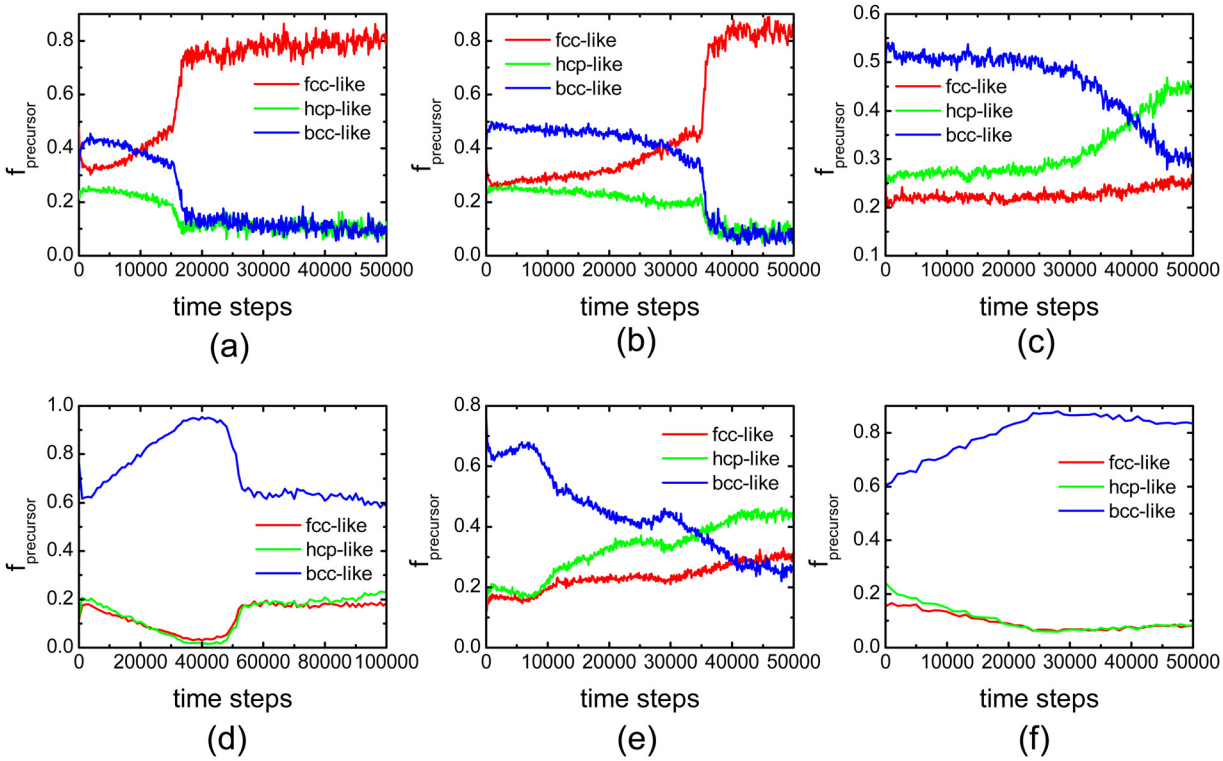

Fig. 9 Temporal fraction of different precursors attached on the surface of the growing crystallite during a typical heterogeneous crystallization process assisted by different structured templates when $\varepsilon = 2$, $\rho = 1.0$. (a) fcc(100) template. (b) fcc(110) template. (c) fcc(111) template. (d) bcc(100) template. (e) bcc(110) template. (f) bcc(111) template. Red, green and blue lines represent the curves of fcc-like, hcp-like, and bcc-like precursors, respectively. Red dashed lines depict the statistic fraction of fcc-like precursors appearing in the MD simulation without templates at the corresponding state point.

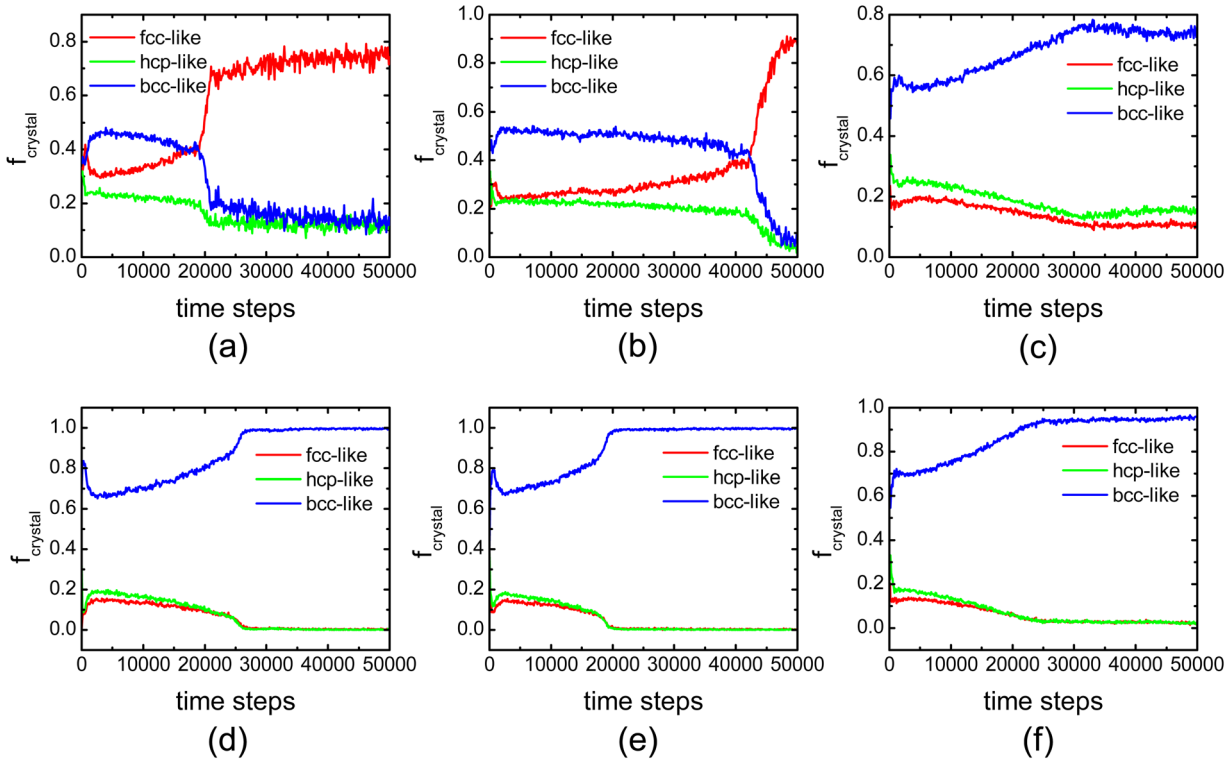

Fig. 10 Temporal fraction of different precursors attached on the surface of growing crystallite during a typical heterogeneous crystallization process assisted by different structured templates when $\varepsilon = 20$, $\rho = 0.55$. (a) fcc(100) template. (b) fcc(110) template. (c) fcc(111) template. (d) bcc(100) template. (e) bcc(110) template. (f) bcc(111) template. Red, green and blue lines represent the curves of fcc-like, hcp-like, and bcc-like precursors, respectively. Blue dashed lines depict the statistic fraction of bcc-like precursors appearing in the MD simulation without templates at the corresponding state point.

the interface thickness of the fcc(100) template is larger but its interface roughness is less. Besides the interface profiles, both the growth rate and the quality of crystals are also influenced by the consistency between the BOO of the crystal surface and BOO of the precursor clusters emerging from the fluid phase. If the orientation order of precursor clusters matches that of the crystal surface, the crystal quality is increased and crystal growth will be boosted.[21,57] As shown in Fig. 9 and 10, the fractional precursors attached on the interface crystal of the fcc(100) template are more than those of the fcc(110) template. Combining all of the factors above, the crystal growth rate of the fcc(100) template is consequently larger than that of the fcc(110) template. Such a physics picture of consistency between BOO of the crystal surface and BOO of the precursors may also explain the fast crystal growth of the bcc(100) template, especially at the state point $\varepsilon = 20$, $\rho = 0.55$.

3.5 Epitaxial crystal growth in charged colloids

Here we briefly describe the dynamic process of template-induced crystallization appearing in charged colloids. Firstly we cool down the liquid phase to below the melting temperature so that the liquid–solid phase transition happens by the thermodynamic driving force. With the assistance of a crystal substrate, the layering crystals form at the location of the substrate and heterogeneous crystallization starts. As the crystallization proceeds, the liquid particles near the liquid–solid interface will become relatively ordered (precursors) and then transform into crystals layer by layer (see Fig. 3 and 4), as if the crystal front moves perpendicular to the template with a cost of the liquid phase.

This picture described above is reminiscent of epitaxial crystal growth which has been widely used to manufacture the thin-film materials for applications in electronics, opto-electronics, and magneto-optics.[58] Referring to the epitaxy techniques which include solid phase epitaxy (SPE), liquid phase epitaxy (LPE), vapor phase epitaxy (VPE) and molecular beam epitaxy (MBE), the template-induced crystallization in this work can be considered to be a LPE of charged colloids as its epilayer phase is liquid. At first glance, the colloidal epitaxy exhibits a layering crystal growth that seems similar to the Frank-van der Merwe mode (FM-mode)[58] in conventional epitaxy. But the epitaxial crystal growth in charged colloids is indeed different from a typical FM mode because the interface has roughness and the crystal front is obviously not an ideal 2D plane (see Table 1). The roughness of crystal front, which has been also found in the epitaxy of some atomic systems (*e.g.*, the atomic epitaxy from melt),[56,59,60] is probably due to the fact that the thermal motions of particles play a nontrivial role (here $k_BT = 1$ that represents the magnitude of thermal motions is comparable to the interaction or potential strength $\varepsilon = 2$ or 20). Although the colloids are usually considered as "big atoms",[3] their properties are actually different from real atoms that are often involved in conventional epitaxy. The motion of colloids

is in principle stochastic rather than deterministic as atoms, but in the MD simulations we do not consider the stochasticity of colloids. Another important difference between the charged colloids and atomic systems is the interaction, which definitely affects the phase behaviors as well as the dynamics of crystal growth. As is known, the charged colloids interact electrostatically and repulsively while the atoms usually interact *via* chemical bonding (*e.g.*, the ionic, covalent and metallic bonding) which is often adhesive. When the surface charge of colloids is low and the interaction strength between colloids is weak, the structure of substrate should match the desired crystal lattice in order to obtain a single crystal with high quality (see Section 3.2). Moreover, the crystal growth rate has a strong dependence on the patterns of substrates, with the largest growth rate for fcc(100) followed by fcc(110) and fcc(111) ones (see Table 1). Such results are in agreement with those of atomic epitaxy from melt.[59,60] When the surface charge of colloids is high and the interaction strength between colloids is strong enough to play a more significant role on the epitaxy, the influence of substrate patterns on the crystal growth is different from that of conventional epitaxy. For the matching fcc-type template, it is no wonder that we achieve similar results to those of atomic epitaxy from melt.[59,60] However, using the bcc-type template we can instead obtain a long-lived metastable and single bcc crystal with high quality (see Section 3.3), which is contradictory with the standard rule of lattice matching in conventional epitaxy.[58]

4. Conclusion

By means of brute-force MD simulation, we have studied template-induced crystallization in charged colloids. Using a large enough number of colloidal particles and implementing a parallel algorithm on the CUDA platform, we can investigate the whole process of heterogeneous crystallization including the layering crystal nucleation and epitaxial growth. In common, the symmetry character of the template plays an important role in the formation of corresponding crystals especially at the early crystallization, *i.e.*, the bcc-type template favors the formation of bcc crystals and bcc-like precursors while the fcc-type template, except the fcc(111) template whose structure benefits not only fcc but also hcp crystals resulting in a similar behavior to homogeneous crystallization, favor the formation of fcc crystals and fcc-like precursors. At different state points (here we consider two typical state points in the fcc region of the constructed phase diagram[43]), the results of heterogeneous crystallization are subtly different correspondingly. When the interaction strength is weak, bcc crystals that are formed with the promotion of bcc-type templates will sooner or later transform into fcc or hcp crystals because they are not stable at all. When the interaction strength is higher (typically $\varepsilon = 20$ and $\rho = 0.55$), the colloidal system can eventually become a crystallite with bcc majority because the bcc crystals cannot transform into thermostatically stable fcc within the time scale of MD simulation. For all the state points, fcc(100) and fcc(110) can help the formation of fcc crystals and those fcc crystals will persist until the end of the crystallization process.

In view of all the results above, we draw a conclusion that if we want a single crystal with high quality, we should use a fcc-type template in most cases where the fcc phase is thermodynamically stable. Definitely, fcc(111) is not a good choice as it always results in a mixture of bcc, hcp and fcc structures. Meanwhile, referring to the estimation of the crystal growth rate which is related to the efficiency of crystal preparation, the fcc(100) template would be the best choice on account of its largest crystal growth rate. When the interaction strength is high, one may use the bcc-type template to induce the formation of metastable bcc crystals on some purpose, but experimentally the bcc crystals will transform into stable fcc finally despite sometimes their lifetime being very long at some state points. Another point we should investigate is the characters of a template, such as the properties of colloidal particles on the template and the lattice length of the patterned template, may not be so ideal in actual experiments. For instance, the properties of charged colloids are influenced by many factors such as its radius, charges on the surface, density of the ion, *etc.*, so the particles on a template are probably different from those bulk charged colloids (heteroepitaxy of charged colloids). All of those mentioned above would be interesting and give a clue for the future and further works.

Conflicts of interest

There are no conflicts to declare.

Acknowledgements

This work was financially supported by the National Natural Science Foundation of China (grant no. 22172180 and 22272191) Programs.

References

1 V. J. Anderson and H. N. W. Lekkerkerker, *Nature*, 2002, **416**, 811–815.
2 D. Frenkel, *Science*, 2002, **296**, 65–66.
3 W. Poon, *Science*, 2004, **304**, 830–831.
4 V. N. Manoharan, *Science*, 2015, **349**, 1253751.
5 U. Gasser, E. R. Weeks, A. Schofield, P. N. Pusey and D. A. Weitz, *Science*, 2001, **292**, 258–262.
6 W. B. Russel, *Nature*, 2003, **421**, 490–491.
7 C. López, *Adv. Mater.*, 2003, **15**, 1679–1704.
8 R. V. Nair and R. Vijaya, *Prog. Quantum Electron.*, 2010, **34**, 89–134.
9 H. L. Cong, B. Yu, J. G. Tang, Z. J. Li and X. S. Liu, *Chem. Soc. Rev.*, 2013, **42**, 7774–7800.
10 X. J. Wu, R. Hong, J. K. Meng, R. Cheng, Z. J. Zhu, G. Wu, Q. Li, C. F. Wang and S. Chen, *Angew. Chem., Int. Ed.*, 2019, **58**, 13556–13564.

11 J. Liu, X. G. Zhang, W. Q. Li, C. Z. Jiang, Z. Y. Wang and X. H. Xiao, *Sci. Chin. Mater.*, 2020, **63**, 1418–1437.
12 S. B. Guo, B. Yu, F. Y. Gao, S. Wang, Y. Q. Shen and H. L. Cong, *J. Ind. Eng. Chem.*, 2021, **96**, 34–58.
13 K. M. Zhu, J. Song, C. Q. Fang, X. Zhou, M. Y. Pu and D. Wang, *J. Mater. Sci. Technol.*, 2023, **141**, 78–99.
14 A. van Blaaderen, *MRS Bull.*, 2004, **29**, 85–90.
15 A. van Blaaderen, R. Ruel and P. Wiltzius, *Nature*, 1997, **385**, 321–324.
16 D. Y. Wang and H. Möhwald, *J. Mater. Chem.*, 2004, **14**, 459–468.
17 N. V. Dziomkina and G. J. Vancso, *Soft Matter*, 2005, **1**, 265–279.
18 S. K. Yang and Y. Lei, *Nanoscale*, 2011, **3**, 2768–2782.
19 H. J. Zhang, S. M. Peng, L. Mao, X. S. Zhou, J. H. Liang, C. B. Wan, J. Zheng and X. Ju, *Phys. Rev. E*, 2014, **89**, 062410.
20 M. Perez-Page, E. Yu, J. Li, M. Rahman, D. M. Dryden, R. Vidu and P. Stroeve, *Adv. Colloid Interface Sci.*, 2016, **234**, 51–79.
21 S. Arai and H. Tanaka, *Nat. Phys.*, 2017, **13**, 503–509.
22 F. C. Meldrum and C. O'Shaughnessy, *Adv. Mater.*, 2020, **32**, 2001068.
23 S. Auer and D. Frenkel, *Phys. Rev. Lett.*, 2003, **91**, 015703.
24 M. Dijkstra, *Phys. Rev. Lett.*, 2004, **93**, 108303.
25 A. Esztermann and H. Löwen, *J. Phys.: Condens. Matter*, 2005, **17**, S429–S441.
26 A. Cacciuto and D. Frenkel, *Phys. Rev. E*, 2005, **72**, 041604.
27 W. S. Xu, Z. Y. Sun and L. J. An, *J. Chem. Phys.*, 2010, **132**, 144506.
28 K. Sandomirski, E. Allahyarov, H. Löwen and S. U. Egelhaaf, *Soft Matter*, 2011, **7**, 8050–8055.
29 S. Dorosz and T. Schilling, *J. Chem. Phys.*, 2012, **136**, 044702.
30 T. Dasgupta, J. R. Edison and M. Dijkstra, *J. Chem. Phys.*, 2017, **146**, 074903.
31 N. Ise and I. S. Sogami, *Structure formation in solution: ionic polymers and colloidal particles*, Springer-Verlag, Berlin, 2005.
32 S. H. Xu, H. W. Zhou, Z. W. Sun and J. C. Xie, *Phys. Rev. E*, 2010, **82**, 010401.
33 K. Kratzer and A. Arnold, *Soft Matter*, 2015, **11**, 2174–2182.
34 W. Z. Ouyang, Z. W. Sun, J. Zhong, H. W. Zhou and S. H. Xu, *Sci. China: Chem.*, 2016, **59**, 316–323.
35 X. Q. Ji, Z. W. Sun, W. Z. Ouyang and S. H. Xu, *J. Chem. Phys.*, 2018, **148**, 174904.
36 M. H. Li, Y. S. Chen, H. Tanaka and P. Tan, *Sci. Adv.*, 2020, **6**, eaaw8938.
37 A. Engelbrecht, R. Meneses and H. J. Schöpe, *Soft Matter*, 2011, **7**, 5685–5690.
38 M. Eshraghi and J. Horbach, *Soft Matter*, 2018, **14**, 4141–4149.
39 Y. L. Zhu, H. Liu, Z. W. Li, H. J. Qian, G. Milano and Z. Y. Lu, *J. Comput. Chem.*, 2013, **34**, 2197–2211.
40 W. Z. Ouyang, B. Sun, Z. W. Sun and S. H. Xu, *J. Chem. Phys.*, 2020, **152**, 054903.
41 T. Soyata, *GPU Parallel Program Development Using CUDA*, CRC Press, Boca Raton, 2018.
42 E. J. W. Verwey and J. T. G. Overbeek, *Theory of the Stability of Lyophobic Colloids*, Elsevier, New York, 1948.
43 F. El Azhar, M. Baus, J. P. Ryckaert and E. J. Meijer, *J. Chem. Phys.*, 2000, **112**, 5121–5126.
44 H. J. C. Berendsen, J. P. M. Postma, W. F. Vangunsteren, A. Dinola and J. R. Haak, *J. Chem. Phys.*, 1984, **81**, 3684–3690.
45 J. Russo and H. Tanaka, *J. Chem. Phys.*, 2016, **145**, 211801.
46 W. Mickel, S. C. Kapfer, G. E. Schröder-Turk and K. Mecke, *J. Chem. Phys.*, 2013, **138**, 044501.
47 J. R. Espinosa, A. Zaragoza, P. Rosales-Pelaez, C. Navarro, C. Valeriani, C. Vega and E. Sanz, *Phys. Rev. Lett.*, 2016, **117**, 135702.
48 W. H. Press, S. A. Teukolsky, W. T. Vetterling and B. P. Flannery, *Numerical Recipes in C: The Art of Scientific Computing*, Cambridge University Press, Cambridge, 2nd edn, 1997.
49 P. R. ten Wolde, M. J. Ruiz-Montero and D. Frenkel, *Phys. Rev. Lett.*, 1995, **75**, 2714–2717.
50 P. R. tenWolde, M. J. Ruiz-Montero and D. Frenkel, *J. Chem. Phys.*, 1996, **104**, 9932–9947.
51 W. Lechner and C. Dellago, *J. Chem. Phys.*, 2008, **129**, 114707.
52 J. Russo and H. Tanaka, *Soft Matter*, 2012, **8**, 4206–4215.
53 W. Ostwald, *Z. Phys. Chem.*, 1897, **22**, 289–330.
54 S. Alexander and J. McTague, *Phys. Rev. Lett.*, 1978, **41**, 702–705.
55 G. Tegze, G. I. Tóth and L. Gránásy, *Phys. Rev. Lett.*, 2011, **106**, 195502.
56 G. Sun, J. Xu and P. Harrowell, *Nat. Mater.*, 2018, **17**, 881–886.
57 Q. Gao, J. D. Ai, S. X. Tang, M. H. Li, Y. S. Chen, J. P. Huang, H. Tong, L. Xu, L. M. Xu, H. Tanaka and P. Tan, *Nat. Mater.*, 2021, **20**, 1431–1439.
58 M. A. Herman, W. Richter and H. Sitter, *Epitaxy: Physical Principles and Technical Implementation*, Springer, Berlin, Heidelberg, 2004.
59 J. Q. Broughton, G. H. Gilmer and K. A. Jackson, *Phys. Rev. Lett.*, 1982, **49**, 1496–1500.
60 M. He, E. T. Karim, M. V. Shugaev and L. V. Zhigilei, *Acta Mater.*, 2021, **203**, 116465.

